

High accuracy verification of a correlated-photon-based method for determining photon-counting detection efficiency

Sergey V. Polyakov and Alan L. Migdall

Optical Technology Division, National Institute of Standards and Technology, 100 Bureau Drive, Gaithersburg, MD 20899-8441 and Joint Quantum Institute, Univ. of Maryland, College Park, MD 20742
sergey.polyakov@nist.gov, migdall@nist.gov

Abstract: We have characterized an independent primary standard method to calibrate detection efficiency of photon-counting detectors based on two-photon correlations. We have verified this method and its uncertainty by comparing it to a substitution method using a conventionally calibrated transfer detector tied to a national primary standard detector scale. We obtained a relative standard uncertainty for the correlated-photon method of 0.18 % ($k=1$) and for the substitution method of 0.17 % ($k=1$). From a series of measurements we found that the two independent calibration techniques differ by 0.14(14) %, which is within the established uncertainty of comparison. We believe this is the highest accuracy characterization and independent verification of the correlated-photon method yet achieved.

©2007 Optical Society of America

OCIS codes: (040.5570) Quantum detectors; (120.3940) Metrology; (270.5290) Photon statistics.

References and links

1. W. H. Louisell, A. Yariv, and A. E. Siegman, "Quantum Fluctuations and Noise in Parametric Processes," *Phys. Rev.* **124**, 1646–1654 (1961).
2. F. Zernike and J. E. Midwinter, *Applied Nonlinear Optics*, (New York: Wiley, 1973).
3. D. C. Burnham and D. L. Weinberg, "Observation of Simultaneity in Parametric Production of Optical Photon Pairs," *Phys. Rev. Lett.* **25**, 84–87 (1970).
4. D. N. Klyshko, "Correlation of Stokes and Anti-Stokes Components under Inelastic Light-Scattering," *Sov. J. Quantum Electron.* **7**, 591–594 (1977).
5. D. N. Klyshko, "On the Use of a 2-Photon Light for Absolute Calibration of Photoelectric Detectors," *Sov. J. Quantum Electron.* **10**, 1112–1116 (1981).
6. A. A. Malygin, A. N. Penin, and A. V. Sergienko, "An Efficient Emission of a Two-Photon Fields in the Visible Region," *Sov. J. Quantum Electron.* **11**, 939–941 (1981).
7. S. R. Bowman, Y. H. Shih, and C. O. Alley, "The use of Geiger mode avalanche photodiodes for precise laser ranging at very low light levels: An experimental evaluation", in *Laser Radar Technology and Applications I*, James M. Cruickshank, Robert C. Harney eds., Proc. SPIE 663, 24–29 (1986).
8. J. G. Rarity, K. D. Ridley, and P. R. Tapster, "Absolute Measurement of Detector Quantum Efficiency Using Parametric Downconversion," *Appl. Opt.* **26**, 4616–4619 (1987).
9. A. N. Penin and A. V. Sergienko, "Absolute Standardless Calibration of Photodetectors Based on Quantum Two-photon Fields," *Appl. Opt.* **30**, 3582–3588, (1991).
10. V. M. Ginzburg, N. Keratishvili, E. L. Korzhenevich, G. V. Lunev, A. N. Penin, and V. Sapritsky, "Absolute Meter of Photodetector Quantum Efficiency Based on the Parametric Down-Conversion Effect," *Opt. Eng.* **32**, 2911–2916 (1993).
11. P. G. Kwiat, A. M. Steinberg, R. Y. Chiao, P. H. Eberhard, and M. D. Petroff, "Absolute Efficiency and Time-Response Measurement of Single-Photon Detectors," *Appl. Opt.* **33**, 1844–1853 (1994).
12. A. Migdall, R. Datla, A. Sergienko, J. S. Orszak, and Y. H. Shih, "Measuring Absolute Infrared Spectral Radiance with Correlated Visible Photons: Technique Verification and Measurement Uncertainty," *Metrologia* **32**, 479–483 (1995/6).
13. G. Brida, S. Castelletto, I. P. Degiovanni, C. Novero, and M. L. Rastello, "Quantum Efficiency and Dead Time of Single-Photon Counting Photodiodes: a Comparison Between Two Measurement Techniques," *Metrologia* **37**, 625–628 (2000).

14. G. Brida, S. Castelletto, I. P. Degiovanni, M. Genovese, C. Novero, and M. L. Rastello, "Towards an Uncertainty Budget in Quantum-Efficiency Measurements with Parametric Fluorescence," *Metrologia* **37**, 629–632 (2000).
15. T. J. Quinn, "Meeting of Directors of National Metrology Institutes held in Sevres on 17 and 18 February 1997," *Metrologia* **34**, 61-65 (1997).
16. A. Ghazi-Bellouati, A. Razet, J. Bastie, M. E. Himbert, I. P. Degiovanni, S. Castelletto and M. L. Rastello, "Radiometric reference for weak radiations: comparison of methods," *Metrologia*, **42**, 271-277 (2005); A. Ghazi-Bellouati, A. Razet, J. Bastie, M. E. Himbert, "Detector calibration at INM using a correlated photons source," *Eur. Phys. J. Appl. Phys.* **35**, 211-216 (2006).
17. for example, J. C. Bienfang, A. J. Gross, A. Mink, B. J. Hershman, A. Nakassis, X. Tang, R. Lu, D. H. Su, C. W. Clark, C. J. Williams, E. W. Hagley and Jesse Wen, "Quantum Key Distribution with 1.25 Gbps Clock Synchronization," *Opt. Express* **12**, 2011-2016 (2004).
18. for example, C. W. Chou, H. de Riedmatten, D. Felinto, S. V. Polyakov, S. J. van Enk, H. J. Kimble, "Measurement-induced entanglement for excitation stored in remote atomic ensembles," *Nature* **438**, 828-832 (2005).
19. M. Ware and A. L. Migdall, "Single-photon Detector Characterization Using Correlated Photons: the March from Feasibility to Metrology," *J. Mod. Opt.* **15**, 1549– 1557 (2004).
20. A. L. Migdall, "Absolute Quantum Efficiency Measurements Using Correlated Photons: Toward a Measurement Protocol," in *Proceedings of IEEE Conference: Transactions on Instrumentation and Measurement*, 50, (IEEE, 2001) 478–481.
21. Determination of the Spectrum Responsivity of Optical Radiation Detectors, Publ. 64 (Commission Internationale de L'Éclairage, Paris, 1984).
22. Budde, W., *Optical Radiation Measurements*, Vol. 4: Physical Detectors of Optical Radiation, (Academic Press, Inc., Orlando, FL, 1983).
23. SPCM-AQR Single Photon Counting Module, product datasheet, available at: <http://optoelectronics.perkinelmer.com/content/Datasheets/SPCM-AQR.pdf>.
24. Perkin-Elmer APD SPCM-AQR-12 (trigger detector: s/n 12432, DUT: s/n 12433)
25. Certain commercial equipment, instruments or materials are identified in this paper to foster understanding. Such identification does not imply recommendation or endorsement by the National Institute of Standards and Technology, nor does it imply that the materials or equipment are necessarily the best available for the purpose.
26. Gamma Scientific Silicon Photodiode p/n: 19830-3 s/n: ND0104
27. M. Ware, A. L. Migdall, J. C. Bienfang, and S. V. Polyakov, "Calibrating Photon-Counting Detectors to High Accuracy: Background and Deadtime Issues," *J. Mod. Opt.*, to appear.
28. S. V. Polyakov, M. Ware, and A. L. Migdall, "High-accuracy calibration of photon-counting detectors", in *Advanced Photon Counting Techniques*, W. Becker, ed., Proc. SPIE 6372 (2006).
29. B. N. Taylor and C. E. Kuyatt, Guidelines for Evaluating and Expressing the Uncertainty of NIST Measurement Results, NIST Technical Note 1297, 1994 Edition.
30. T. C. Larason, S. S. Bruce, and A. C. Parr, Spectroradiometric Detector Measurements, Part 1–Ultraviolet Detectors, and Part 2–Ultraviolet and Visible to Near-Infrared Detectors, NIST Special Publication 250-41.
31. S. W. Brown, G. P. Eppeldauer, and K. R. Lykke, "Facility for spectral irradiance and radiance responsivity calibrations using uniform sources," *Appl. Opt.* **45**, 8218-8237 (2006)
32. M. M. Choy and R. L. Byer, "Accurate 2nd-order Susceptibility Measurements of Visible and Infrared Nonlinear Crystals," *Phys. Rev. B* **14**, 1693-1706 (1976).
33. Establishing transmittance with desired accuracy requires temporal stability of associated irradiance measurements. The experimental setup consisted of a He-Ne laser followed by a spatial filter (pinhole), and two trap detectors with a high degree of spatial uniformity. One trap detector monitored the laser's power and the other measured the transmitted power with and without the crystal. The maximum observed long-term drift of the system was 0.004 %/h, and the rms of the signal, normalized to laser power, was 0.02 %.
34. J. Cheung, J. Gardner, A. L. Migdall, S. V. Polyakov, and M. Ware, "High Accuracy Lens Transmittance Measurements," submitted to *Appl. Opt.*

1. Introduction

We present the implementation of a single-photon detector (SPD) calibration procedure based on detection of (correlated) photon pairs produced by parametric downconversion (PDC). The method, because it is a fundamentally absolute way to calibrate SPD detection efficiency (DE) [1-14], has been described as a "primary standard method." [15] The absolute nature of the method derives from the two-photon light source. Because the photons are produced in pairs, the detection of one photon heralds with certainty the existence of the other. Because the method relies on individual photons as a trigger, the scheme operates directly in the photon-

counting regime and is thus well suited to single-photon count measurements. For some time, this method has promised high accuracy calibrations, however, progress has been slow and true independent verifications have been lacking. While relative standard uncertainties better than 1 % have been reported recently [13, 14, 16], the correlated photon method has not been independently verified to that level of uncertainty. The effort presented here addresses this deficiency by making such a measurement and comparison at high accuracy. To allow this method to achieve its promised potential and to be used with confidence, it is critical to have such high accuracy verifications. This effort is particularly timely as there are a number of areas where well characterized photon counting detectors are increasingly required, such as quantum communication [17] and quantum state measurements [18]. This growing need is also evidenced in the number of new commercial offerings of photon-counting detectors for these applications.

To assess the correlated photon calibration technique and verify its claimed uncertainty, we perform a high accuracy two-photon calibration of a photon-counting detector and an independent calibration by comparison to a conventional photodiode, whose calibration is traceable to the National Institute of Standards and Technology's (NIST) absolute reference cryogenic radiometer-based spectral responsivity scale. An important property of our measurement protocol is that the SPD output for the two calibration methods is collected simultaneously minimizing the comparison uncertainty.

2. Calibration methods

2.1 Correlated-photon-pair calibration method

The correlated-photon method relies on a fundamental property of parametric down-conversion, namely, that photons from a pump beam are split into two photons (signal and idler), whose frequencies, and wavevectors are governed by energy conservation and momentum conservation, respectively. Therefore, detection of one photon of a correlated pair, provides both spatial and temporal location information of the other photon of the pair. To make a detection efficiency measurement, a trigger SPD is set to intercept some of the downconverted light. The single-photon detector under test (DUT) is positioned to collect all the photons correlated to those seen by the trigger detector. The DUT channel detection efficiency is the ratio of the number of coincidence events to the number of trigger detection events in a given time interval (assuming that the detectors only fire due to photons of a pair). A coincidence is defined as when both the trigger and the DUT detectors fire within a given time window due to detection of both photons of a downconverted pair. If we denote the detection efficiency of the DUT and trigger channels by η_{DUTchan} and η_{trigchan} , respectively, then the total number of trigger counts is

$$N_{\text{trig}} = \eta_{\text{trigchan}} N \quad (1)$$

and the total number of coincidence events is

$$N_c = \eta_{\text{DUTchan}} \eta_{\text{trigchan}} N, \quad (2)$$

where N is the total number of down-converted photons seen by the trigger channel during the measurement period. The absolute detection efficiency of the DUT channel is

$$\eta_{\text{DUTchan}} = N_c / N_{\text{trig}}, \quad (3)$$

which is independent of η_{trigchan} . Thus, measurements of the trigger channel collection efficiency, and calibration of the trigger SPD are unnecessary. Note that η_{DUTchan} is the efficiency of the entire detection channel, including collection optics and filters, not just the efficiency of the DUT alone [19, 20]. To determine the efficiency of the DUT, denoted by η_{DUT} , from η_{DUTchan} , all losses in the DUT path before reaching the DUT have to be included. The total channel transmittance is a product of transmittances of individual optical

elements in the DUT path. Transmittance values, along with the methods and uncertainties of their measurement, are considered below.

2.2 Conventional Calibration (Substitution method)

The substitution method is used to independently measure the detection efficiency of the SPD. The method as used here, relies on measuring the radiant power of the DUT channel with a standard detector (traceable to NIST's radiant power scale) and with the photon-counting DUT [21, 22]. To compare the radiant power measured by the standard detector to number of counts measured by the SPD, requires information about the spectrum of the source and specifics of the SPD itself.

3. Calibration setup

The experimental setup seen in Fig. 1 is used for both the conventional and correlated measurements. The signals from Trigger and DUT SPDs are collected by a circuit that records both the overall number of trigger and DUT events, and the correlation between trigger and DUT events in the form of a histogram with 0.1 ns temporal resolution. Because the coincidence events used for the two-photon calibration and the count rate of the DUT used for the conventional calibration are recorded simultaneously, the two types of calibrations are effectively made simultaneously. To complete the substitution method, the DUT SPD is replaced with a calibrated detector. For all measurements the pump power was monitored.

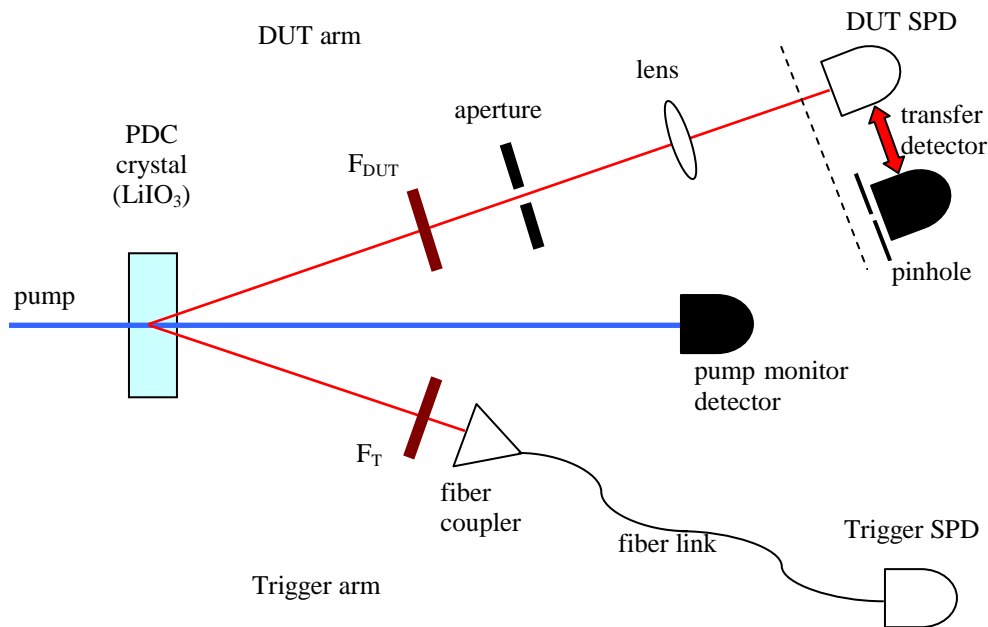


Fig. 1. Calibration setup.

In our setup, a 351 nm Ar^+ laser line pumps the downconversion crystal. A windowless silicon photodetector monitors the pump power. A LiIO_3 crystal (6 mm long) was set to produce nearly degenerate downconverted photons at about 702 nm in a non-collinear phase-matching configuration with an output angle of 1.8° (air) with respect to the pump beam. The sensitivities of the trigger and DUT photon-counting modules peak at ≈ 700 nm [23]. The trigger detector, a photon-counting avalanche photodiode (APD) module, was set at the end of a 5 m single-mode fiber. The DUT detector was also a photon-counting avalanche photodiode module mounted behind an aperture to reduce PDC light not correlated to that seen by the trigger and a lens to collect the correlated light onto the ~ 0.2 mm DUT active area. The

independently calibrated transfer standard photodetector, a cooled high-shunt resistance Si PIN photodiode, was mounted for easy interchange with the DUT. In addition, a pinhole mounted close to the Si PIN photodiode's surface was used to restrict wings of the illuminating beam. Although the wings contain a small fraction of the beam power, it becomes relevant at our level of uncertainty.

3.1 Implementation of the correlated photon pair calibration method

To minimize the uncertainties associated with the correlation method, the photons paired with those detected by the trigger SPD must be delivered to the DUT SPD with low loss. Therefore, the following guidelines should be followed:

- the spectral band of the filter F_T should be narrow enough to select a small portion of the photons created by the downconversion process.
- the spectral band of F_{DUT} should completely encompass the correlated band defined by F_T , which in practice means that the band of F_{DUT} is significantly wider to guarantee the overlap, but narrow enough to avoid saturation of the DUT. The shape of the bandpasses should be as rectangular as possible and have minimal fringing.
- the aperture in the DUT arm should let through virtually all of the photons correlated with ones detected by a trigger arm, while restricting the number of uncorrelated photons that would otherwise land on the DUT.
- the lens should collect all the light correlated to the light seen by the trigger channel.

An accurate experimental determination of N_{trig} requires the electronic detector pulses to be summed during the counting period, and relevant corrections applied. Corrections include darkcounts and counts due to background photons, that are independently measured. Other corrections deal with imperfections in the SPD and its electronics, as well as in the pulse and coincidence counting electronics. These corrections require estimates of quantities such as the fraction of afterpulses in the trigger arm, double-back reflection of the fiber link which delays a trigger pulse resulting in a reduction of the main coincidence peak, and the fraction of histogram measurements that are cut short due to retriggering of the start channel. Experimental techniques for estimating some of these corrections are reviewed in Ref. [20].

We determine N_c from a histogram (see Fig. 2) of the delays between trigger and DUT detection events. This histogram contains the main correlation peak, along with other correlated features that result from various properties of the SPD used along with peculiarities of the setup. After the main coincidence peak the most obvious features are due to afterpulsing and deadtime. The correlated signal "sits" on top of a background of uncorrelated coincidences. To separate the signal and background with the precision needed for the ultimate detection efficiency determination, a detailed model of APD behavior [24, 25] is required. Finally, to extract the detection efficiency of the SPD from the detection efficiency of the entire DUT channel, all the optical losses in the DUT path must be determined. These losses are: the Fresnel reflectance loss of the output surface of the PDC crystal, the loss of the filter F_{DUT} , the loss of the lens, and the loss due to the finite size of the aperture [25]. Note that the insertion loss due to F_{DUT} depends on spectral distribution of the correlated photons, which is related to the filter F_T by the energy conservation constraint of the downconversion phenomenon.

3.2 Implementation of a substitution method

To implement the second independent calibration method, we collect the rate of single-photon detections in the DUT arm, and correct for darkcounts and afterpulsing of the DUT APD. It is important to note that afterpulsing is more likely if a photon is absorbed by the APD during the last ≈ 10 ns of its deadtime. This effect, referred to as twilight time, is due to nonideal biasing pulse shapes [24]. It is important to distinguish between an afterpulse resulting solely from an earlier firing of the detector (the usual definition of the term) and a pulse resulting from a subsequent photon absorption during the twilight time. The fraction of afterpulsing due to each of these effects must be determined.

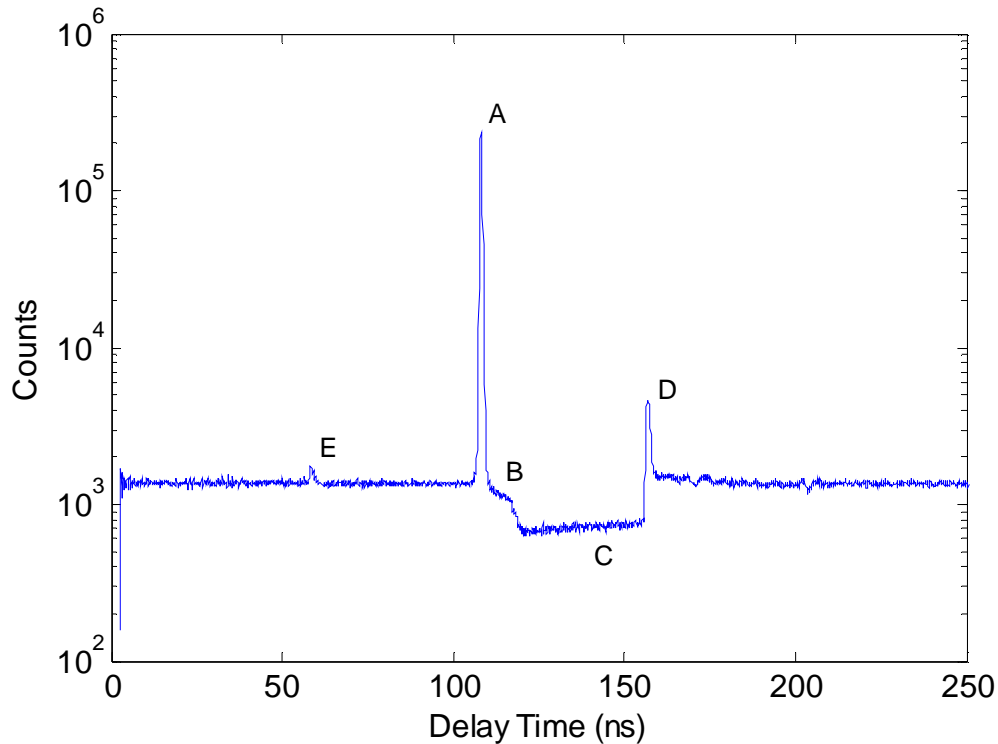


Fig. 2. Typical histogram and its main features. A – the main peak due to correlated photons, B – extended shoulder due to twilight events (see text), C – the region where the detector is dead after firing, D – peak due to afterpulsing, E – minor correlated photons peak due to double back reflection in the trigger fiber and afterpulsing of the trigger APD. The broad background is due to the uncorrelated firing of the DUT.

Because the active area diameters of the APD (≈ 0.2 mm) and the calibrated photodetector (5.8 mm) are very different, a 0.2 mm diameter pinhole aperture is used with the larger detector (Fig. 1). This aperture is used to exclude any stray light that may surround the central beam configured to underfill the 0.2 mm diameter APD active area. Because of the large difference in detector active area, even a very low intensity beam wing when integrated over that additional detector area could significantly affect the final results.

To complete the comparison of the two detectors' measurements we must convert radiant power into photon flux. This is achieved by integrating the spectral responsivity of the detector with the spectrum of light after the filter. This spectrum is governed by the F_{DUT} bandpass and the PDC source spectrum, approximated as a white light source.

Finally, to correct for laser power fluctuations as the sequential detector substitutions are made, the pump power is monitored for normalization purposes. We note that this is required for the substitution comparison, not for the correlated photon efficiency determination which is not directly sensitive to pump power.

4. Calibration results and uncertainty budget

4.1 Definition of APD detection efficiency

Here, we introduce a definition of DE for our APD-based SPD that allows for a high accuracy comparison between the two methods, which is the overall goal of this work. This definition allows for real-life APD features such as deadtime, afterpulsing, and twilight counts. [24] Because of the complicated nature of photon-counting detectors, the definition of DE often depends on the particular application. For example, if an application ignores delayed

detections, the resulting DE definition must reflect this condition. Here, we define DE as the history independent probability that an APD will produce an electrical pulse given one photon incident on its surface. By “history independent,” we mean that the resulting DE is an average DE made at a particular mean incident photon rate. As defined, the APD’s DE will vary with count rate due to deadtime effects. Also, this definition includes all delayed detections which can range up to ≈ 10 ns beyond the usual propagation delay.

4.2 Comparison of correlated photon pair and substitution calibration methods

The comparison consisted of a set of measurements made over two days, where the APD DUT and calibrated photodiode were alternately swapped into the setup. (The APD DUT measurements, which included correlated and single-photon counts, provided data for both independent calibration methods simultaneously.) The duration of each run was chosen to accumulate enough data to obtain a statistical uncertainty at or below 0.1 % ($k=1$ is used for all uncertainties herein unless otherwise stated). After each detector swap, the horizontal and vertical position of the active area was verified and, if necessary, adjusted. Four conventional calibration runs were taken each day. Because of power variations of the pump laser, it was necessary to normalize the conventional calibrations. This normalization allowed the correlation calibration data to be compared against all the conventional runs of that day. To compare the calibrations performed by two independent methods, the DE of the APD was determined from each of the 4 datasets and is presented in Fig. 3. We see that while the DE values for each APD trial are different, the agreement between correlated and conventional methods is excellent.

The difference from run to run of the DUT DE is due to two reasons. First, the DUT APD has significant nonuniformity of response across its detection area making it difficult to exactly reproduce the DUT position between swaps. Second, following our definition of DE, its value has some dependence on count rate. While it is possible to introduce corrections for deadtime, APD twilight properties, etc., the comparison experiment would suffer from additional uncertainties if we were to undertake such corrections, negating the overall goal of this effort. Because of these concerns, our efforts consist of comparisons between the substitution method and the correlated method of fixed positions on the detector at a specific count rate, rather than comparison between repeated measurements taken under different conditions.

We note that the comparison procedure derives the DEs from photon flux values taken during different runs of the conventional photodetector which shows some fluctuation (within their respective confidence bands) during the day. Similar fluctuations are seen on the two separate days. One of the possible causes of such behavior may be a thermal effect on a filter F_{DUT} , however, since the measured values stay well within their respective confidence bands, no further investigation was undertaken.

The relative uncertainty of the detector substitution determination of DE is found to be 0.17 %. The relative uncertainty of the correlated method is found to be 0.18 %, which compares favorably to 0.5%, the best previously reported uncertainty for this method [13,14]. These results allow for a single run comparison of the two methods to ≈ 0.25 %.

We define the agreement between the two independent calibration methods as

$$\Delta = \frac{\bar{\eta}_{DUT,conventional} - \eta_{DUT,correlated}}{(\bar{\eta}_{DUT,conventional} + \eta_{DUT,correlated})/2}, \quad (4)$$

where $\bar{\eta}_{DUT,conventional}$ is an average DE over each group of 4 calibrated detector runs for a fixed position of an APD. The uncertainty of the comparison is found from the individual uncertainties of the two methods. Figure 4 shows Δ along with confidence bands ($k = 1,2$) for all trials.

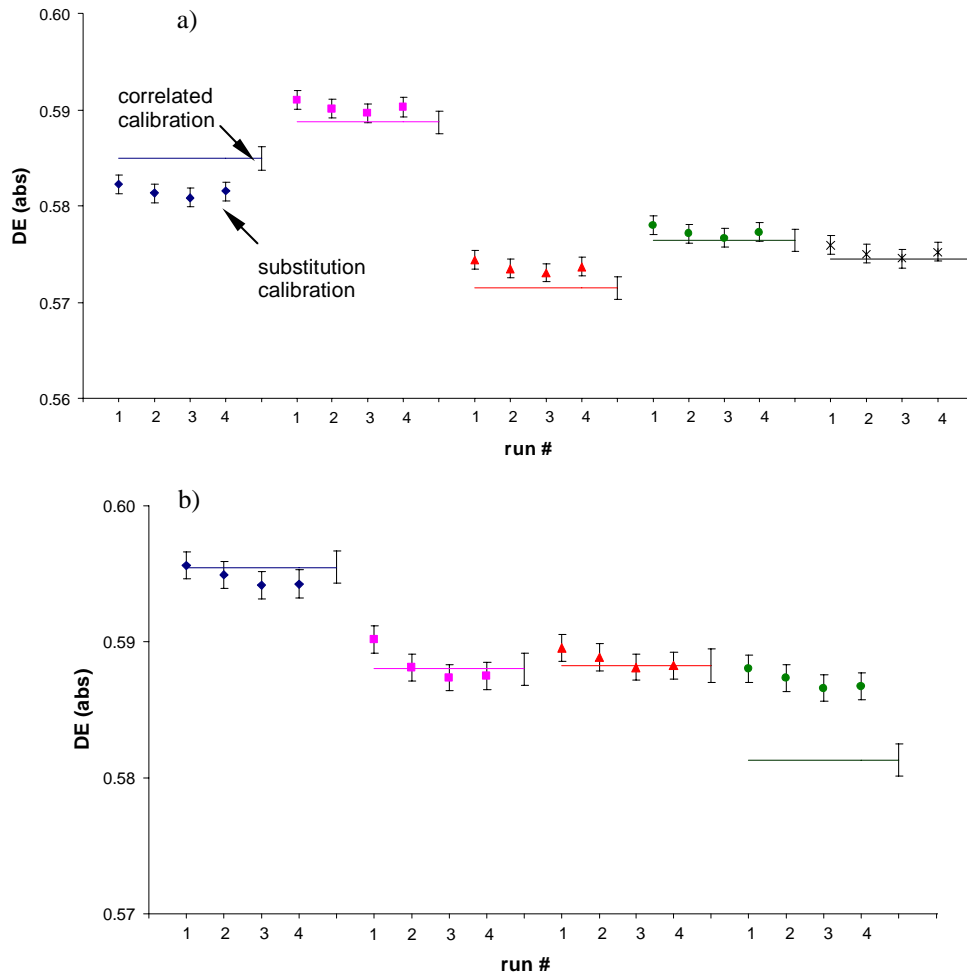


Fig. 3. DEs determined from four substitution calibration runs (points) are compared to DEs determined by correlated calibration (lines). Each comparison is for slightly different areas of the DUT and incident photon rates. a) calibration day 1; b) calibration day 2.

We see that differences between the two methods of calibration presented in Fig. 4 are distributed between the confidence bands as would be expected for a normal distribution with 6 out of the 9 measurements falling at or within $k=1$ of zero [26]. We further find that the mean difference between the two methods is 0.14 %, while the uncertainty of this mean is 0.14 %. Thus, the mean difference between the two methods is comparable to the uncertainty of the comparison, supporting the equivalence of the two absolute calibration methods, limiting any residual bias to the level of the uncertainty of the comparison. Note that we reduce the uncertainty of the comparison between methods by repeating the verification experiment, until the systematic component of uncertainty dominates. This is a 7-fold improvement over the best previously reported independent verification of 1% [12]. We believe that this is the highest accuracy verification of the correlated photon method yet reported.

4.3 Uncertainty budget

An overview of uncertainty budget is presented in Table 1 for the conventional, detector substitution based, calibration method and Table 2 for the correlated photon pair method. The total uncertainty for each method is combined in quadrature to obtain the uncertainties shown

in Fig. 3. The combined uncertainty of a comparison is the quadrature sum of the two final values given in Tables 1 and 2 and shown in Fig. 4. See the Appendix for how their uncertainties were estimated.

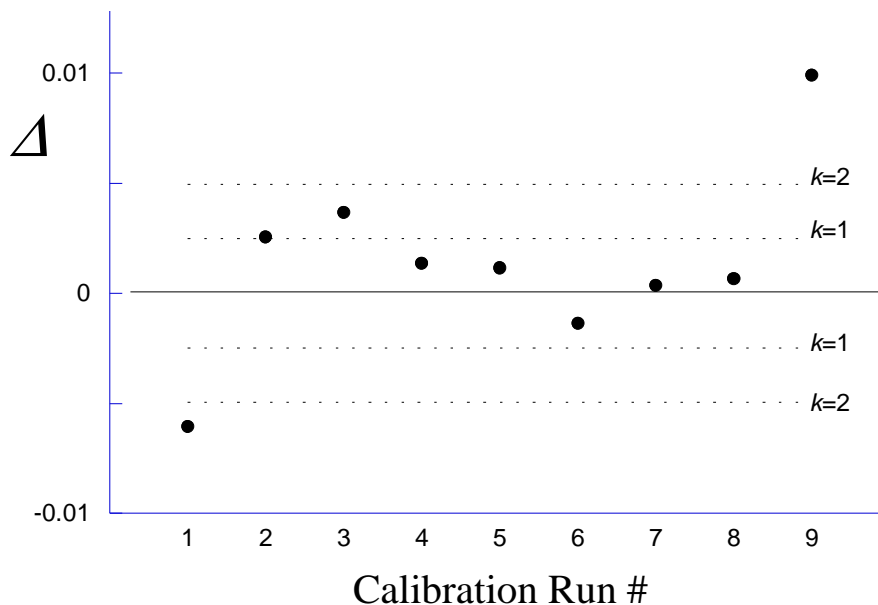


Fig. 4. Comparison between two absolute calibration methods: correlated photon pair and substitution (traceable to NIST scale). The size of the confidence bands reflects the uncertainty of each individual comparison and indicates the consistency of the overall comparison with zero bias between the two methods.

5. Conclusion

We have implemented a calibration experiment that provides for two high accuracy primary standard calibration methods for SPDs: a correlated photon calibration method with 0.18 % absolute uncertainty and a detector substitution method, traceable to the NIST radiant power scale, with 0.17 % absolute uncertainty. Comparison of the two methods allowed us to perform, a high accuracy verification of the correlated photon calibration method. We found that the two independent calibration methods differ by $0.14 \% \pm 0.14 \%$ with the uncertainty of individual comparison of 0.25 %. Both the uncertainties of these individual calibrations and the uncertainty of the comparison between the two calibration methods significantly surpass previously reported efforts. These comparison results and component analyses improve the understanding of experimental techniques associated with photon counting using SPDs and thereby allow the correlated photon calibration method to be used with confidence.

Acknowledgements

For their numerous invaluable contributions without which such an involved metrology project could never have been undertaken, we thank Joshua Bienfang, Steve Brown, Jessica Cheung, Sergio Cova, George Eppeldauer, Gerald Fraser, Jeanne Houston, Tom Larason, Keith Lykke, Dave Plusquellic, Eric Shirley, and Michael Ware.

This work was supported in part by DTO, ARO, and DARPA/QUIST.

Table 1. Detector substitution (conventional) calibration uncertainty budget

Physical property	Value	Relative uncertainty of value (%)	Sensitivity	Relative uncertainty of DE (%)
Analog transfer standard calibration (QE equivalent)	0.61906	0.10	1	0.10
Spatial nonuniformity of photodiode at 700nm, (standard deviation of central responsivity)	1	0.025	1	0.025
Analog measurement statistics & drift				0.06
Analog amplifier gain calibration at 10^{10} V/A	1.0022	0.050	1	0.05
Pinhole backside reflection	0	0.10	1	0.10
DUT signal & background statistics				0.003
DUT afterpulsing	0.00322	11.6	0.003	0.04
DUT deadtime (due to rate changes with time)				0.02
Total				0.17

Table 2. Correlated photon calibration method uncertainty budget

Physical property	Value	Relative uncertainty of value (%)	Sensitivity	Relative uncertainty of DE (%)
Crystal reflectance	0.09249	0.2	0.1	0.02
Crystal transmittance	0.99996	0.009	1	0.009
Lens transmittance	0.9753	0.02	1	0.02
Geometric collection (from raster scan)	0.9995	0.04	1	0.04
DUT filter transmittance	0.9136	0.10	0.91	0.09
Trigger bandpass to virtual bandpass wavelength				0.07
Histogram background subtraction				0.03
Coincidence circuit correction	0.0083	10.0	0.008	0.08
Counting statistics				0.07
Deadtime (due to rate changes with time)				0.022
Trigger afterpulsing	0.0025	25.0	0.003	0.06
Trigger background, & statistics	175000	0.3	0.035	0.01
Trigger signal due to uncorrelated photons	0			0.033
Trigger signal due to fiber back reflection	0.00202	1.60	0.002	0.003
Total				0.18

Appendix: Independent measurements of physical properties of the setup

A.1 Analog transfer standard calibration

The conventional photodetector used in the detector substitution tests was independently calibrated with a relative uncertainty of 0.1 % ($k=1$) as described in [27] and traceable to NIST's cryogenic radiometer-based radiant power scale. The detector was a windowed Si photodiode cooled to achieve a shunt resistance above 3 G Ω to allow for high gain and low

noise. The detector was integrated with a current-to-voltage amplifier. The detector/amplifier package was calibrated at a gain of 10^7 V/A and was used at a gain of 10^{10} V/A for the detector substitution measurements.

Because the photodiode was calibrated for radiant power, a conversion was needed to obtain a DE value. An interpolation of the radiant power responsivity spectral dependence was done over the F_{DUT} bandpass region and weighted with the transmittance function of F_{DUT} . For this calculation, we assumed an ideal white light source illuminating the DUT channel. To assess the effect of this assumption the actual emission spectrum of our PDC source was measured. The weighted responsivities using the white light assumption and the measured spectrum were compared. Because the measured detector responsivity fit well to a linear function, a linear interpolation was chosen with a resulting uncertainty of 0.002 %.

An issue in determining the shape of F_{DUT} was the effect of interference fringing when measuring its transmittance with a monochromatic laser. F_{DUT} was measured with NIST's Spectral Irradiance and Radiance Calibrations with Uniform Sources (SIRCUS) facility with an uncertainty of 0.1 % [28]. A fringe amplitude of ~ 0.5 % is evident along with some drift of the phase of that fringe over time (see Fig. 9(a)). The effect of the fringe was determined by mathematical modeling (where fringe phase was varied) and its resulting effect on the final DE determination was found to be small, $\sim 2 \cdot 10^{-5}$ %. The absolute transmittance of F_{DUT} does not contribute to the final DE uncertainty, because only the bandpass shape, not its absolute transmittance is used in the calibration. Also, the contribution due to the wavelength uncertainty of SIRCUS (0.01 nm) is small, $\approx 10^{-4}$ %. One final uncertainty to be considered here is due to the transmission tails of F_{DUT} . This is estimated to be $\approx 2 \cdot 10^{-4}$ %. Thus, the dominant contribution to the uncertainty is the independent photodetector calibration of 0.1 %, with all the other uncertainties small enough to be neglected. The final value for the spectrally weighted DE of the photodiode used for the substitution method is 0.61906.

A.2 Spatial uniformity (at 700nm)

The spatial uniformity of the conventional photodetector was measured as part of the calibration procedure (see [27]). The standard deviation of the spatial variation of responsivity near the center of the detector was ~ 0.025 %.

A.3 Analog measurement statistics & drift

Each conventional photodetector run consisted of interleaved signal and background measurements to correct for any long-term drift. A typical relative uncertainty for the (signal – background) was found to be 0.06 %

A.4 Analog amplifier gain calibration

Our substitution measurements were performed at a gain setting of 10^{10} V/A. Given the shunt resistance of a few $\text{G}\Omega$ of our cooled detector, this was the highest practical gain setting. The 10^{10} V/A gain setting was calibrated relative to the 10^7 V/A gain at which the detector was calibrated. The calibrated gain factor was found to be 1.0022 times the nominal gain ratio of 1000 with a relative uncertainty of 0.05 % by comparing outputs as gains were changed while detector input was held constant.

A.5 Pinhole backside reflection/scatter

Because the reflectance of the conventional photodetector is quite high (~ 30 %), light trapping can significantly affect these measurement results. Of particular initial concern was the 0.2 mm diameter pinhole aperture used to reduce the effective detector area of the 5.8 mm diameter photodiode (see Fig. 1). The back of the aperture was blackened to minimize any scattered/reflected light off of the photodiode from coupling back into the photodiode. Variation of the aperture-detector distance showed (Fig. 5) that the magnitude of any residual backscatter was less than the 0.1% measurement uncertainty.

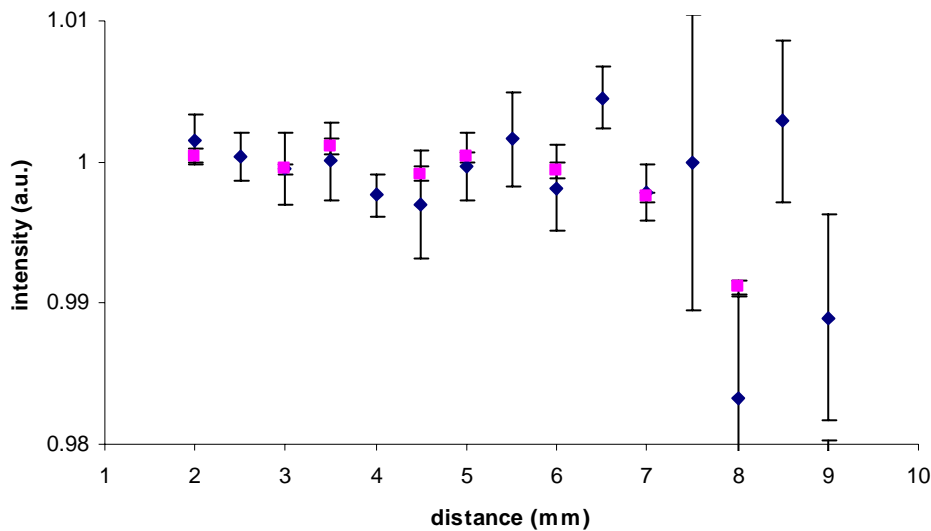


Fig. 5. Looking for evidence of backside scatter from a closely placed pinhole and its effect on the conventional photodetector measurements. Signal is shown as the detector was moved away from the masking pinhole. Two experimental datasets are shown, one with small uncertainty (squares) showing zero slope at short distances and one with larger uncertainty (diamonds) confirming the falloff at large distances.

A.6 DUT signal and background statistics

DUT background events must be subtracted from the DUT signal events to obtain the DUT DE. Signal and background were collected in 10 s interleaved measurements with the background being ≈ 3500 counts/10 s, while the signal was $\approx 3 \cdot 10^7$ counts/10 s. In a single 10 s measurement the statistical uncertainty of the background is 2 %, with the sensitivity of the calibration to the background level being 0.0012, contributing a 0.002 % uncertainty to the final calibration. The signal uncertainty is 0.02 %, with a sensitivity of unity. Typical measurements consisted of at least 50 such 10 s measurements reducing these already small uncertainty contributions by more than a factor of 7 to 0.003 %.

A.7 DUT afterpulsing

An afterpulse is when the APD fires (produces a count) at the end of the deadtime associated with a previous count. In addition to the usual cause of an afterpulse due to lingering trapped carriers from a previous avalanche, an afterpulse can also result from a subsequent photon arriving during the last moments of the APD's deadtime [24]. Thus the afterpulse peak consists of photon-related afterpulses (or twilight counts) and ordinary afterpulses, not related to a photon absorption. Our definition of an APD DE includes all twilight events as valid, while discarding ordinary afterpulses. Note that the ordinary afterpulse fraction is a property of a specific APD, in that it varies from unit to unit and does not depend on count rate. At the same time, the probability of getting a twilight event grows approximately linearly with increasing count rate. With count rates larger than ≈ 50 kHz, twilight counts noticeably affect the calibration result. Considering the high DUT count rates in our measurements (more than 3 MHz), a separate set of measurements was used to quantify the levels of ordinary and twilight afterpulses. By measuring the afterpulse fraction (defined as the likelihood of an afterpulse given an initial count of the detector producing a second pulse not due to a second photon) at a range of DUT count rates, we can quantify and fit the linearly growing component of the twilight count rate. The slope of the resulting line is proportional to the duration of the twilight period and associated "twilight detection efficiency" (which might not

be a constant throughout this interval). The zero rate intersection of this line is the ratio of ordinary afterpulses. Measurements of the DUT APD (Fig. 6) yielded an ordinary afterpulsing fraction of $0.003218 \pm 11.6\%$. This translates to a 0.04 % contribution to the uncertainty budget.

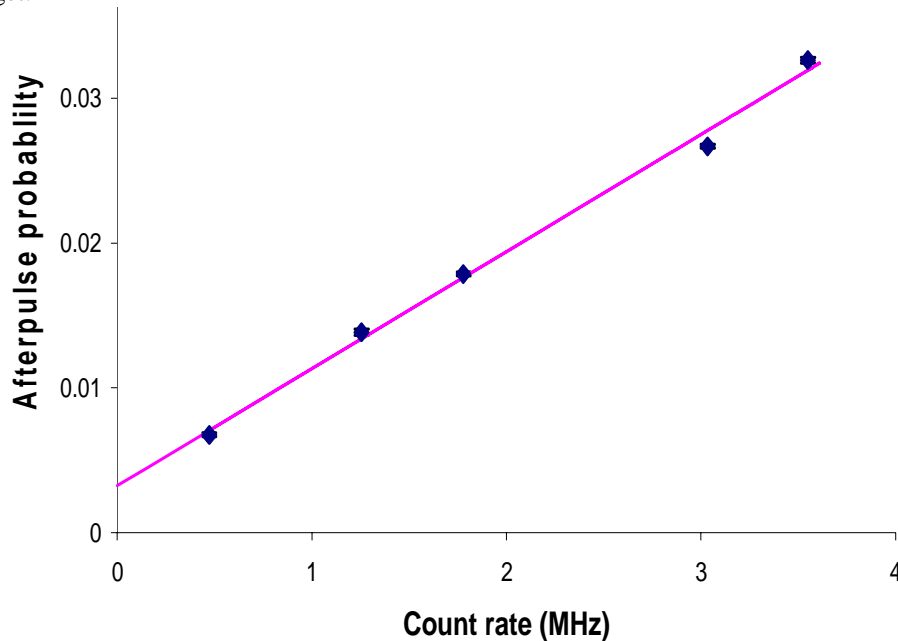


Fig. 6. Afterpulsing of the detector under test APD at various count rates. Uncertainty bars are shown.

A.8 DUT deadtime

Because the DE of the APD (see above) is count-rate dependent and our final DE is averaged over a range of rates, we must estimate the APD DUT linearity. The count rate changes predominantly because of pump laser power drift, which is estimated to be 3 % root mean square (rms). The DE variation is mainly due to nonzero deadtime of the APD, ≈ 50 ns. This variation is estimated by the formula [23]:

$$C_{\tau=0} = \frac{C_{\text{measured}}}{1 - \tau C_{\text{measured}}}, \quad (5)$$

where τ is the deadtime interval, C_{measured} is the measured count rate, and $C_{\tau=0}$ is the hypothetical zero deadtime rate. Comparing the difference in actual rates produced with a constant radiant pump power, versus a varying power of $\approx 3\%$ rms, we find a difference of 0.022 % for a typical 3 MHz count rate and 50 ns deadtime.

A.9 Crystal reflectance

The crystal's single surface Fresnel reflectance is determined by experiment and theory. The theoretical results are used in our uncertainty estimate; the experiment, which could not be easily done at the required precision, served as a check on the theory and verified that the crystal surface was not damaged.

The theoretical reflectance was computed using refraction data taken from a published Sellmeier fit [29]. The angle of incidence between the beam direction and the crystal surface was measured to be $1.7(1)^\circ$ using He-Ne laser. The resulting calculated reflectance coefficient was 0.092488 with an estimated uncertainty of 0.2 % (of value) due to the finite spectral band of the measurement, as well as the spatial extent of the source region and the angular spread

subtended by that region as viewed by the collection system. The low overall DE sensitivity factor is ≈ 0.1 , because the experiment is directly sensitive to the crystal transmittance which is $\approx 10x$ larger than reflectance. This low sensitivity to angle variation translates to a DE uncertainty component of 0.02 %.

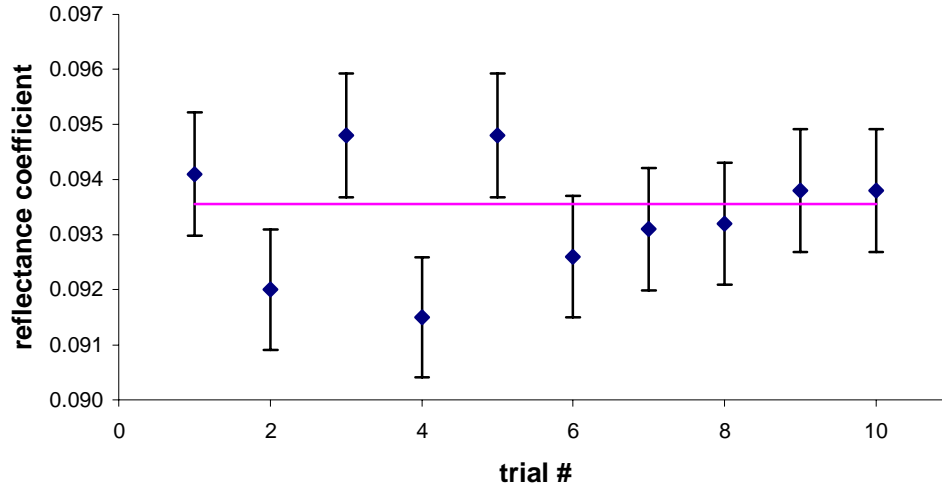


Fig. 7. Reflectance measurements (points) and calculation (line) for LiIO₃ at 632.8 nm at incidence angle of 1.7°.

The experimental verification of the crystal surface reflectance was done with a He-Ne laser beam aligned to the angle of incidence of the correlated photons in our setup. The reflectance coefficient was obtained from the ratio of transmitted and incident power with the transmitted beam including multiple order reflections. The single surface transmittance, T , is found from the measured external transmittance, T_{measured} by

$$T_{\text{measured}} = T^2(1 + (1 - T)^2). \quad (6)$$

This formula for incoherent light was used because the overlap between subsequent order reflections was small. We see that the calculation and the measurement agree to well within the uncertainty of 0.1 % (Fig. 7). Figure 7 is used only to illustrate the accuracy of our calculations, the actual reflectance coefficient used in our calibration at 702 nm was 1.1 % lower than the 632.8 nm result due to dispersion. In addition to this transmittance measurement, a direct reflectance measurement was also made which was consistent with the calculation, but with greater uncertainty than the transmittance result.

A.10 Crystal transmittance

In addition to reflectance loss at the output of the downconversion crystal, any absorptive loss within the crystal must also be determined. The LiIO₃ crystal is highly transparent with absorption resonances at wavelengths much shorter than 500 nm, so minimal absorptance is expected at the wavelength range of interest, i.e. 700 nm. However, crystal defects may lead to some residual absorption (or scattering). Because crystals differ in quality, we independently characterized the crystal used in our experiment. To put a limit on the crystal absorption, we measured its transmittance with a He-Ne laser at 632.8 nm, and compared it to the calculated transmittance assuming only Fresnel losses based on published refractive index data [29]. Because these crystal defect induced losses should not depend on wavelength in the region of crystal transparency, the 632.8 nm result should apply also to 702 nm. The measured

value of the transmittance of the crystal is 0.82917 ± 0.00016 , whereas the calculated value assuming only Fresnel losses is 0.82924 ± 0.00002 . This result demonstrates that the loss in the crystal is negligible: $(0.7 \pm 1.7) \cdot 10^{-4}$. Hence the crystal transmittance is $(99.993 \pm 0.017) \%$. While this small absorptance is for the entire internal crystal length, the downconverted photons on average travel through only half of the length, so the effect of this already small value is further reduced by a factor of 2. Hence, the effective transmittance is equal to $(99.996 \pm 0.009) \%$.

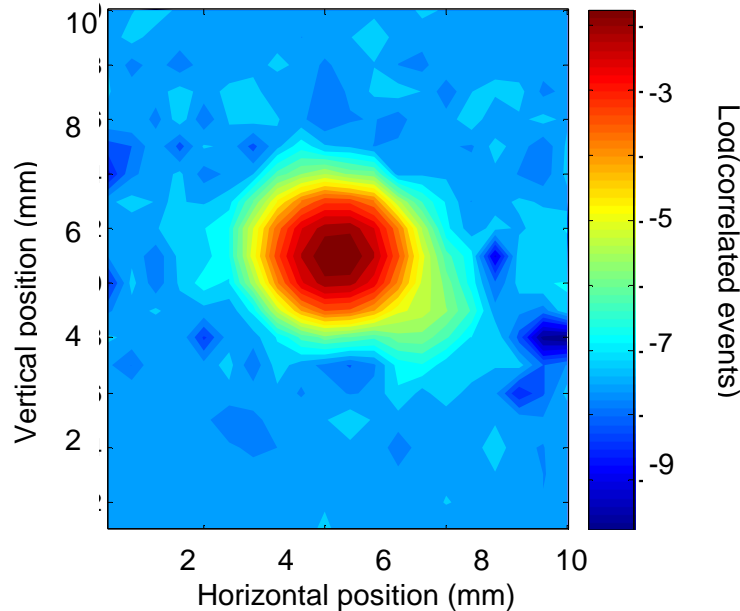


Fig. 8. Spatial map of the log of correlated counts at the DUT, as the entire DUT arm with a 1 mm aperture was scanned across the beam. Evidence of a secondary spot due to double reflection is visible below and to the right of the main spot. (Due to noise on the background a constant was added to the counts after background subtraction, but before taking the log.)

A.11 Lens transmittance

The transmittance of the lens ($f=19$ mm and anti-reflection coated) used in the DUT arm was independently determined using the method described in [30]. The measured transmittance was equal to $(97.53 \pm 0.02) \%$.

A.12 Geometric collection (raster scan test)

The correlated technique requires that all the photons correlated with those coupled to the single-mode fiber of the trigger arm be collected by the DUT, as any geometric losses would contribute to reduction of the apparent overall DE. By scanning the DUT arm with a small diameter (~ 1 mm) aperture, we mapped the spatial distribution of the correlated counts. In Fig. 8, we see a hint of a secondary spot due to a double reflection on the crystal to the lower right of the main spot. The fraction of correlated photons in this spot is $\sim 1 \%$ of the total. With this beam shape, centering the 6 mm diameter aperture (which was used for the calibration) on the peak would result in a loss of $\sim 0.05 \%$ of the correlated counts, of which approximately 0.01 % of the counts are lost from the main peak, and about 0.04 % are lost due to partial clipping of the weak peak. Hence the correction factor due to this collection loss is 0.9995 with an uncertainty of 0.05 % estimated by allowing for a 0.25 mm misalignment of the correlation peak and the aperture.

A.13 DUT filter transmittance

To compute absolute losses of the DUT channel requires the absolute F_{DUT} transmittance spectrum. The measurements of this spectrum were performed on the NIST SIRCUS system [28] with a relative uncertainty of 0.1 %. Two measurements taken 1 hour apart are presented in Fig. 9(a). Note that the fringe on top of the spectrum shifts during the day, presumably due to thermal effects. We found that because the transmittance coefficient for the correlated photons requires the spectral shape of the DUT filter to be integrated with the trigger arm bandpass, the resulting DE uncertainty due to a shifting fringe is less than 0.1 %. This calculation is addressed next.

A.14 Trigger bandpass to virtual bandpass

Because of energy conservation, the spectral band of the DUT DE measurement is set by the trigger arm bandpass (i.e. effectively creating a virtual DUT bandpass filter for the correlated photons). To calculate this virtual bandpass of the DUT for those photons correlated with the photons detected by the trigger, we measured the spectral transmittance shape of the trigger filter and used this information to obtain weights for summing over the DUT transmittance shape. We estimated the uncertainty associated with possible fringe instability (due to thermal effects) on each of the filters. Transmittance for the trigger filter was also measured using SIRCUS, (Fig. 9(b)). The overall transmittance of the virtual DUT bandpass was found to be 0.9136. The uncertainty of this value comes from the two sources: the first is the accuracy of the SIRCUS measurement itself already addressed. The second uncertainty element arises from possible phase shifts in the fringe component of the two spectra. We estimated the effect of this fringe phase shift by fitting the measurements of both filters to a function with an oscillating component and varying the phase of that oscillation. The results showed that this produced a 0.07 % standard deviation of the resulting transmittance as the phases of the two filter fringes were varied. Also, the uncertainty due to the wavelength uncertainty of the SIRCUS apparatus was estimated to be $3 \cdot 10^{-3}$ %.

A.15 Histogram background subtraction

We estimated the uncertainty due to the histogram background subtraction, Fig. 2, by two methods. First, we used the standard deviation of the individual bins in the histogram background window preceding the coincidence peak and calculated an uncertainty of the mean. This yielded an uncertainty of the coincidence minus background result of 0.03 % for our data runs which were timed to produce $\approx 1.8 \times 10^6$ coincidence counts.

A similar result is obtained by assuming that the histogram background obeys Poisson statistics, so that its standard deviation equals the square root of the observed events. This estimation yields the same uncertainty to within 10 %. The agreement of these two methods indicates that the noise on the number of counts in each bin is due to photon statistics rather than to systematic variation of bin size.

A.16 Coincidence circuit correction

The coincidence circuit used to make our correlated measurements produced histograms of “stop” events, with each histogram distribution run triggered by a single “start” event. The circuit is designed to record all stops after the start trigger pulse, unless a subsequent start arrives, that aborts the histogram before recording all stops out to the time limit of the histogram range. In addition to this designed operation, some additional histograms appear to end prematurely ~ 50 ns after starting. The cause of this effect is not understood, but its magnitude was studied and estimated. The typical background floor in the absence of a correlated signal was measured and the fraction of dropped runs was estimated at the location of the correlation peak. For a trigger channel count rate of 11 kHz, typical of our calibration measurements, the fraction of dropped counts is 0.83 %. This value is count rate dependent, and the uncertainty associated with this correction is dominated by the variation of count rate of the trigger channel. Our estimation of the uncertainty is 10 % of the value. The overall

contribution of this uncertainty to the DE calibration is reduced by the sensitivity ratio of 0.008, and equals 0.08 %.

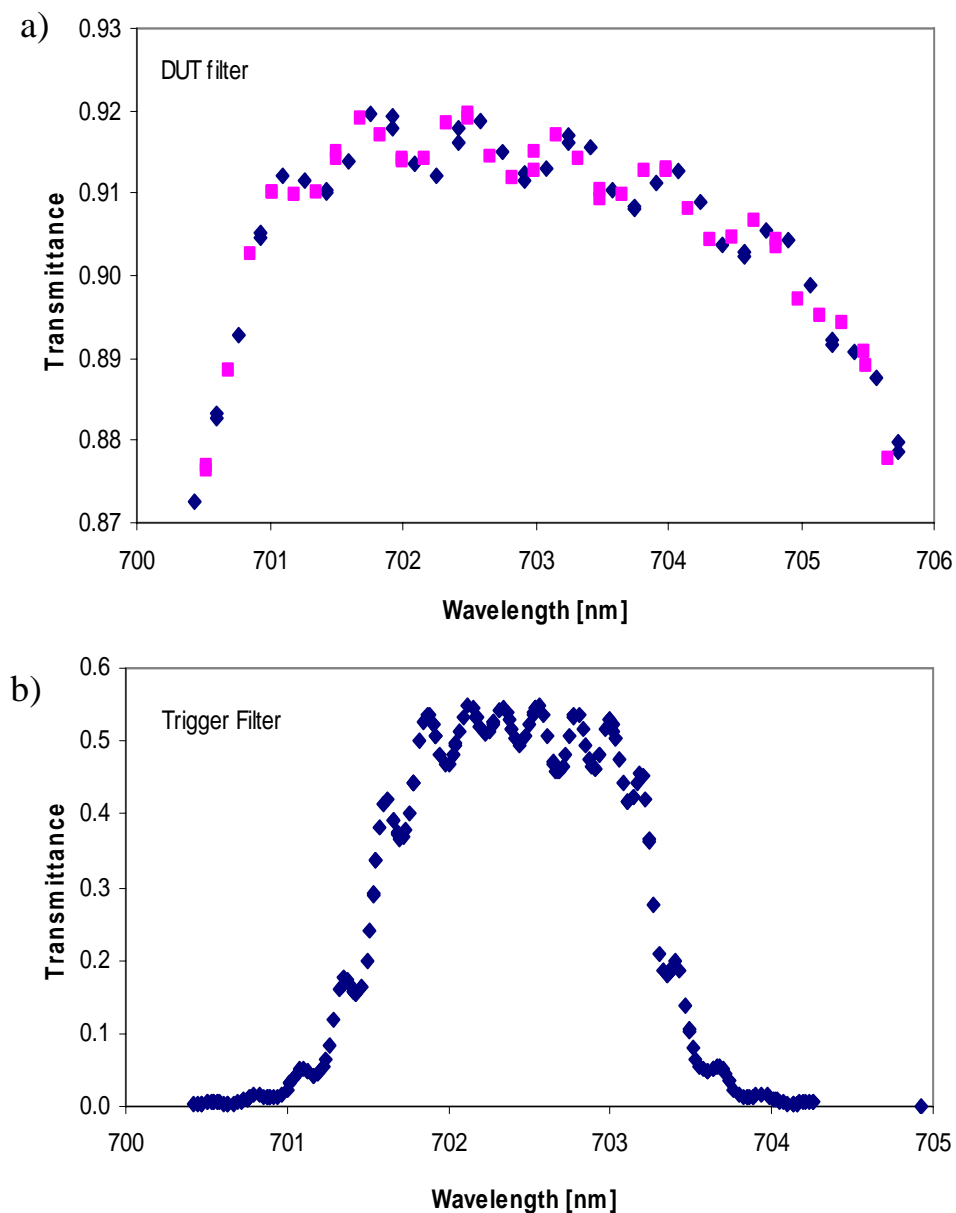


Fig. 9. Transmittance spectra of filters measured with SIRCUS. a) FDUT: two measurements (squares, diamonds) taken ~1 hour apart. b) FT.

A.17 Counting measurement statistics

Each correlated photon calibration run consisted of a series of 10 s measurements with the total number of counts kept at $\approx 1.8 \times 10^6$, yielding a photon-counting statistical uncertainty of 0.07 %.

A.18 Trigger afterpulsing

To measure the afterpulsing on a trigger detector, the electrical part of the experimental setup was rewired as follows: the signal from the trigger APD was sent to a stop channel of the coincidence circuit with an added delay (instead of the usual 'start' channel), and the DUT APD was directed to the start input. The signal in DUT arm was attenuated to reduce the count rate. The measured ratio of the ordinary afterpulsing rate in the trigger channel to the total trigger rate was 0.25 %. The uncertainty associated with this measurement is higher than for the DUT afterpulse measurement, because the rate of starts is significantly higher than the rate of stops. The uncertainty of this measurement is 25 %, contributing an uncertainty of 0.06 % to the final DE determination.

A.19 Trigger background, & statistics

The background subtraction for the trigger APD does not differ conceptually from DUT background subtraction discussed earlier. As before, the total background collected in 10 s amounts to ≈ 3500 counts, yielding a 2 % standard deviation for a single 10 s measurement, however, the trigger signal is lower and the sensitivity of the overall measurement is higher (0.035), so the uncertainty associated with this subtraction for the usual run of 50, 10 s measurements is somewhat higher (0.01 %).

A.20 Trigger signal due to uncorrelated photons

Any trigger channel counts arising from photons not part of a correlated pair must be subtracted from the trigger total before determining the DE by Eq. 3. To determine the portion of photons due to uncorrelated light, we rotate the pump beam polarization by 90° which destroys the phase matching and turns off the downconversion process. Any remaining signal is due either to photon pairs produced by imperfect polarization of the rotated pump beam or scatter due to uncorrelated light. Because this measurement reduces the coincidence rate by a factor of ≈ 500 , while the uncorrelated scatter should remain unchanged, we would expect the effect of the scatter to be greatly magnified. To look for this effect, we measured the total number of trigger counts and the corresponding number of correlated counts of the APD DUT, and compared them using Eq. 3 with the efficiency η_{DUTchan} established by our calibration. We also establish the uncertainty of these measurements. Using these measurements and uncertainties, we found the comparison to be consistent with the assumption that there was no uncorrelated photon scatter in our trigger channel to within our measurement limits. The uncertainty of this comparison is equal to the uncertainty in the determination of N_{trig} ($\approx 10\%$) and N_c ($\approx 4\%$) added in quadrature, but because the correlated signal is attenuated by about 500 times, this limits the uncorrelated trigger signal to $< 0.033\%$.

A.21 Trigger signal due to double back reflection in the fiber

The size of the double-reflection of the fiber link used in a trigger channel together with the trigger APD was independently measured. This reflection is expected to create a small, but significant echo of delayed correlated photons in a trigger channel. To make this measurement, a fast laser diode (at 850 nm) was coupled into the fiber from free space and the output of the APD was connected to a reverse start-stop time-stamping acquisition board. The laser trigger was used as the stop and the APD output as the start. In this setting, the board requires a stop before it can accept another start, so no afterpulsing of the APD can be recorded. The mean measured fiber reflectance value is 0.202(3) %, a relative uncertainty of 1.6 %. Because the sensitivity to fiber reflection uncertainty on the overall DE determination is 2×10^{-3} , the contribution of this uncertainty contribution is $3.2 \times 10^{-3}\%$.